

**APPLICATION OF LONG-DISTANCE FORWARD-SCATTERING PARTICLE IMAGE VELOCIMETRY
IN MICRO-SCALE TURBULENT JET FLOW TESTS**

Lichuan Gui, Bernard J. Jansen and John M. Seiner

National Center for Physical Acoustics (NCPA), University of Mississippi
University, MS 38677, USA

ABSTRACT

A new particle image velocimetry system is applied to measure turbulent air jet flows from a micro-scale nozzle. The applied MPIV system includes a long-distance microscope that enables not only a long working distance, but also a forward-scattering optical setup. By using a high repeating rate Nd:YAG laser and an advanced digital camera, particle image recordings can be captured at 60 fps, i.e. 30 PIV recording pairs per second, with an interframing time of 180 ns, so that a high-speed flow measurement is enabled in micro scale. Measurements were conducted in the central plane of an air jet from a nozzle of 500 μm in diameter at flow velocity up to 110 m/s. Mean velocity and Reynolds stress distributions were determined with statistical analyses of thousands of instantaneous velocity maps.

INTRODUCTION

Since 1998, micro-scale particle image velocimetry (MPIV) has been used in several areas, e.g. aerospace, computer, automotive, and biomedical industries, to determine flow fields in micro-fabricated fluidic devices, see Wereley et al. (2002a). The first MPIV system was presented by Santiago et al. (1998) that was capable of measuring very slow flows, i.e. velocities on the order of tens of microns per second, with a spatial resolution of $6.9 \times 6.9 \times 1.5 \mu\text{m}$. The applications of the MPIV technique moved steadily toward faster flows by replacing the originally used Hg-arc lamp with a two-headed Nd:YAG laser that allowed cross correlation analysis of singly-exposed image pairs acquired with sub-microsecond time intervals between images in each pair. Meinhart, et al., (1999) applied MPIV to measure the flow field in a $30 \times 300 \mu\text{m}^2$ rectangular channel, with a flow rate of 50 $\mu\text{l/hr}$, equivalent to a centerline velocity of 10 mm/s. A subsequent investigation by Meinhart and Zhang (2000) of the flow inside a microfabricated ink jet printer head yielded a high speed measurement of up to 8 m/s. More MPIV application examples were presented by Tkaczyk et al (2002), Lee et al (2002, 2004), Wereley et al (1998, 2002b). Because of the seeding difficulty and high magnification, the MPIV technique were limited to determine liquid flow fields of low Reynolds numbers.

In the presented work, the authors tried to extend the capability of the MPIV technique to measure micro-scale, high-speed flows of gaseous phase, which are generally unsteady and turbulent. In order to access the gaseous flow with minimal disturbance, a long working distance is essential. Among commercially available long-distance microscopes, the QUESTAR QM 100 is currently the best to fit the goal, i.e. it has a field of view of 0.41 mm with a 2/3" format camera at a working distance of 15 cm, and especially, it has an annular lens that enables a zero-degree, forward-scattering configuration to achieve maximal scattered light intensity. Many different kinds of smoke have been used to visualize air flows; however, few of them are used as seeding particles in PIV tests, because the smoke particles are usually too small to be imaged in macro-scale. A incense smoke was used here to seed the micro-scale air flow, because it can be easily obtained and is not harmful when released in small amounts into the open air. The MPIV system used in this work includes a double-head Nd:YAG laser of high repeating rate (30-Hz for each laser head) and a camera with a short interframing time (180 ns), to capture a large number of recording pairs in each test case of relatively high-speed flow. An individual particle image pattern tracking algorithm described by Gui et al. (1977) was improved and used to determine the particle image displacements. An irregular median filter was used to validate the velocity vectors. A statistical analysis was applied to obtain mean and turbulent values of the measured jet flows.

EXPERIMENT SETUP

A schematic illumination of the experimental setup is given in Fig 1. The measurement system includes a double-head, New Wave Solo II-30 Nd:YAG Laser that generates 532-nm, 30 Hz pulses from each of the two laser heads. The laser pulses have a 3-5ns duration, and the pulse energy can be adjusted from a very low level up to 30mJ. The 2.5-mm, pulsed laser beam is aligned into the axis of the microscope lens and the camera, and it goes across the micro-scale air jet. A Questar QM 100 long-distance microscope is focused at the cross-section of the air jet flow and the laser beam with a field of view of around $1 \times 1 \text{ mm}^2$ at a

distance of 120 mm. The scattered light of the particles in the jet flow was collected through an annular window into the microscope. The light collection window has an outside diameter of 60 mm, and the area within its 22-mm inside diameter is not transparent, and it blocks the laser light passing through the jet flow. A Cooke PCO2000 camera that has a 14-bit dynamic range and a 4-GB image memory was used to record 30 particle image recording pairs per second with an imaging scale of $0.94 \mu\text{m}/\text{pixel}$. A BNC 565 multi-channel digital delay/pulse generator was used to synchronize the laser pulses and the digital camera. The control of the camera and the image acquisition were accomplished with a lap-top computer. Fresh air was pumped into a chamber of $17 \times 17 \times 12 \text{ cm}^3$ with an aquarium pump, the flow rate is controlled with a miniature valve. The sandalwood incense

available in many Asian stores was burn in the chamber as a source of tracer particles. The smoke-air mixture was then lead to the test model with a standard aquarium airline tubing. The pressure difference between the chamber and the open environment is monitored with a U-tube pressure gauge. The test model had a 7 cm^3 cylindrical plenum chamber to achieve a calm condition before entering the jet. The jet nozzle is a cylindrical tube of $500 \mu\text{m}$ in diameter and 8 mm in length. The air in the model chamber was accelerated by the pressure difference between the chamber and the open environment to form a high-speed jet flow at the nozzle exit. During the tests the temperatures in the burning chamber and the environment were 42°C and 27°C , respectively.

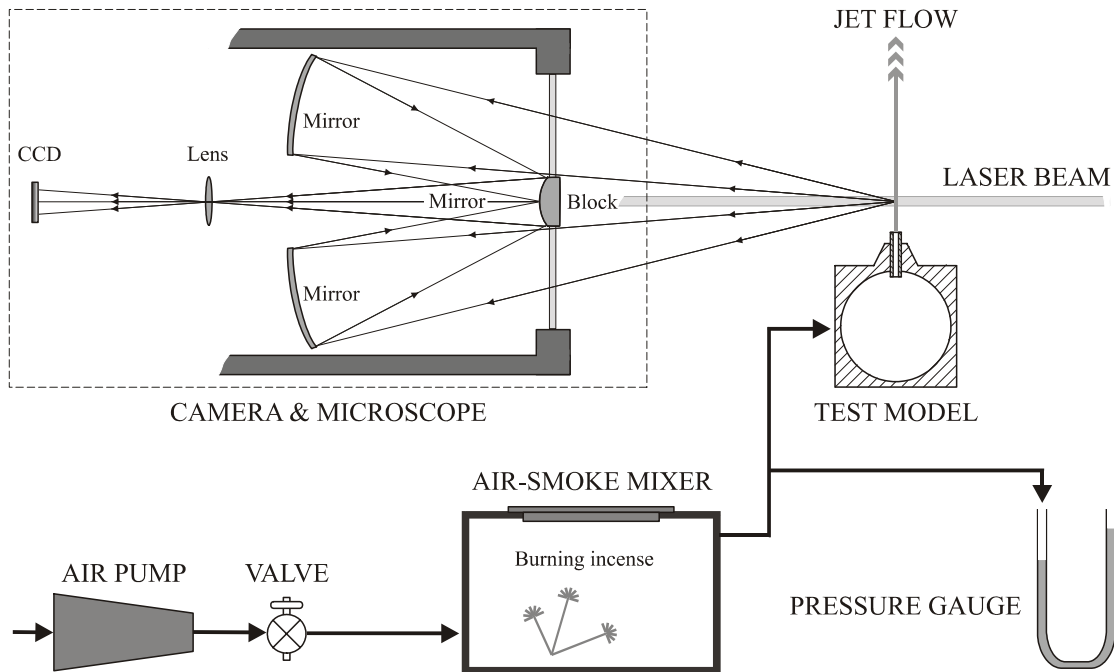


Fig. 1: Schematic illumination of the experimental setup

In the presented work, tests were conducted to map the mean velocity and Reynolds stress distributions in the center plane of a jet flow at three different locations, i.e. $0.5D$, $1.5D$ and $2.5D$ downstream (nozzle diameter $D=500 \mu\text{m}$). The incense smoke particles were obviously smaller than usual particles seeded in air flow because they cannot be imaged individually with a standard PIV system. In the current tests the object-to-image ratio was set to $0.94 \mu\text{m}/\text{pixel}$ to obtain the optimal particle image size, i.e. 3 pixels in diameter. The image frame was set to 1024×256 pixels to achieve the highest recording rate (i.e. 30 pairs per second). The corresponding field of view was $960 \times 240 \mu\text{m}^2$. The time interval between two laser pulses was set to 200ns. The reading of the pressure gauge was controlled around $1000 \text{ mmH}_2\text{O}$ to overcome the resistance in the micro tube and obtain a high speed jet flow of more than 100 m/s . The 4GB image memory of the camera was divided into 3 partitions for the three test potions, respectively, so that 1676 image recording pairs were acquired for each position. The image acquisition for each test position was completed in one minute, whereas it took about 30 seconds

to switch the test positions. During the roughly 5-minute test period, the pressure gauge kept a constant value. As an example, a part of an image pair in size of 240×240 pixels is shown in Fig. 2 that displays a very low particle image number density. The average distance between particle images is much larger than the particle image displacements that were around 20 pixels in the jet center. The particle images taken in current tests have an optimal image size (around 3 pixels) and a very good contrast. However, the same as in conventional M-PIV tests, some particles out of the test plane were also imaged in the recording as background noise.

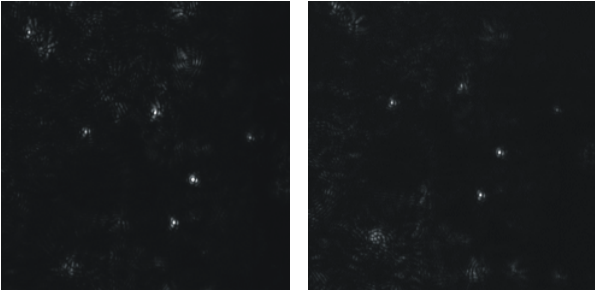


Fig. 2: Part of an image pair (240×240 pixels)

PARTICLE IMAGE PATTERN TRACKING

A low-image-density (LID), singly exposed particle image recording pair can be evaluated by using an individual particle image pattern tracking method with the followed steps:

- (1) Enhance the contrast of particle images by removing a background image or by using a digital filter;
- (2) Determine position of each particle image center in the first frame of the particle recording pair;
- (3) Select an image pattern of each particle in the first frame by placing a small interrogation window at the particle image center position;
- (4) Track the selected image pattern in the second frame to determine the particle image displacement.

The basic idea of the individual particle image pattern tracking was presented by Gui et al. (1977). In step (1) the background image can be obtained either by taking an image in the measurement flow without seeding, or by averaging a group of LID recordings. The determination of particle image position in step (2) can be completed in a very simple way, i.e. by searching for local maxima over a given gray value threshold. The interrogation window in step (3) should be small enough to include only one particle image to achieve a maximal spatial resolution. In step (4) an image pattern tracking scheme based on the correlation-based continuous window shift (CCWS, Gui and Werely 2002) was adopted to replace the originally introduced MQD method (Gui and Merzkirch 1996) to achieve a higher accuracy. The image pattern tracking method is described below:

1. Estimate an initial particle image displacement or set it to zero;
2. Shift the interrogation window with the estimated particle image displacement to determine the tracked image pattern in the second frame;
3. Correlate the gray value distributions of the two image patterns;
4. Determine the high-peak position of the correlation function with sub-pixel accuracy;
5. Add the value of the correlation high-peak position to the estimated particle image displacement;
6. Repeat until the high-peak position has converged.

The criterion to terminate the iteration in step 6 is determined from the required precision and the data processing time. Usually the particle image displacement converges after 5 iterations, however, an iteration number limit should be set to avoid an unlimited loop when the computation does not converge.

The result of the individual particle image pattern tracking in a pair of PIV recordings taken in the air jet flow at $1.5D$ is given in Fig.3 (a), which demonstrates randomly distributed velocity vectors. Because of the low particle image number density, the instantaneous velocity vector map does not provide much information to describe the measured flow. Therefore, multiple recordings are necessary for the current tests. Fig. 3 (b) displays velocity vectors of overlapping 100 individual vector maps, in which enough information is available in the main jet flow but a lack of information still exists at the edge and out of the jet flow. In the following, all the 1676 vector maps in each recording group are used to complete the statistical analysis.

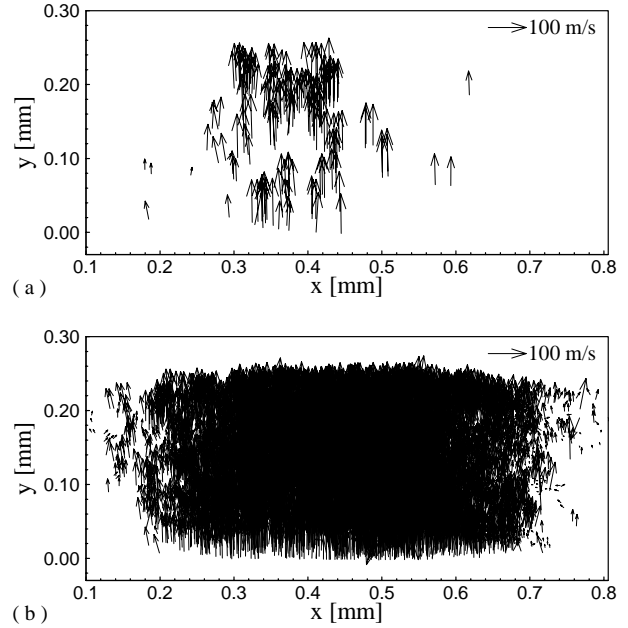


Fig. 3: Evaluated raw vector maps: (a) a single vector map; (b) overlapped 100 vector maps.

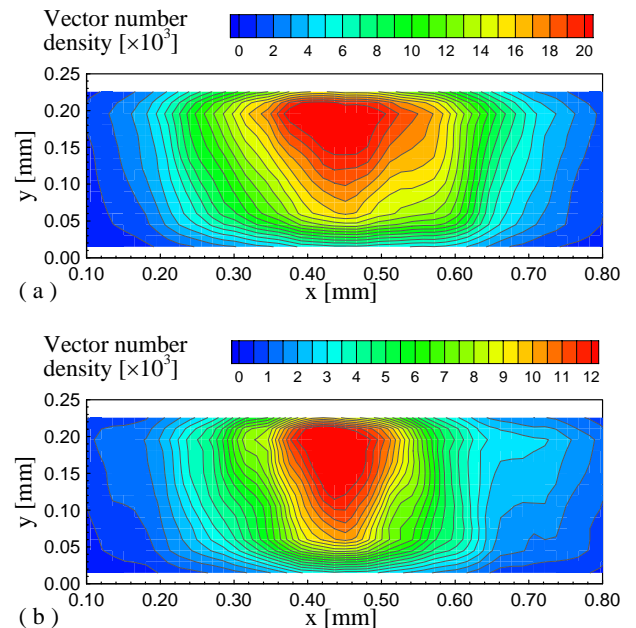


Fig. 4: Vector number density (vector number in a 32×32-pixel window) for test at 1.5D: (a) raw vectors; (b) valid vectors.

DATA VALIDATION AND PROCESSING

Assume a group of randomly distributed raw vectors is recorded as $\{(x_i, y_i, u_i, v_i); i=1,2,3, \dots, N\}$, wherein x_i, y_i are position components; u_i, v_i are velocity components; and N is the total number of the raw vectors in the group. A median filter is applied to test the validation of the raw vector at each position in the following way: First, a sub-group of raw vectors is selected in a circular region centered at (x_i, y_i) with radius r_o . Then the median values of both velocity components are determined in the sub-group of raw vectors as (u_m, v_m) . Finally, the vector at (x_i, y_i) , i.e. (u_i, v_i) , is compared to the median vector (u_m, v_m) . The vector is considered as a valid vector when the difference is not more than a given tolerance value ε , i.e.

$$(u_i - u_m)^2 + (v_i - v_m)^2 \leq \varepsilon^2 \quad (1)$$

Median filter radius r_o is determined according to velocity gradient and the vector number density, i.e. small enough to avoid obvious velocity gradients in the selected region and big enough to include sufficient number of vectors. At least 3 vectors are required to determine a median vector, and the median filter only works when the reasonable vectors outnumber the erroneous vectors.

The described median filtering usually requires substantial computation time, especially with several hundred thousand raw vectors. An effective way to accelerate the median filtering is to divide the whole field into square or rectangular sub-regions. A median vector is determined in each sub-region and compared to every raw vector in the sub-region, so that the erroneous vectors can be identified with criterion in Eq.(1) and removed. The size of the sub-region is determined according to velocity gradient and the vector number density. If a rectangular sub-region is used, the long axis should be oriented to the direction of lower velocity gradient. In the following tests the filtering was conducted with 32×32-pixel sub-regions. Fig. 4(a) shows the raw vector number density, which is defined here as raw vector number in a 32×32-pixel window, for test case at 1.5D. The raw vector number density has a maximum of 11000 at the center of the jet, whereas it is very low out of the main jet flow, because no special seeding was applied in the environment flow. As an example of the median filtering results, Fig. 4(b) shows the valid vector number density, i.e. valid vector number in a 32×32-pixel window. In this test case the valid vector number density has a maximum of 9000 in the jet flow center, but it reduces to a minimum of 360 out of the main jet flow. The total raw vector number and the valid vector number are 802412 and 559259, respectively, i.e. 30% of raw vectors are identified as erroneous vectors with the irregular median filtering. The high rate of erroneous vectors results from the out-of-plane particle images because of the volume illumination. The variation of vector number density along the jet flow axis can be explained that the light intensity is not uniform across the diameter of the laser beam.

A statistical analysis was conducted with the randomly distributed valid vectors to obtain mean velocities and turbulent values with a regular grid distribution. The regular grid for the

final results was determined so that the expected details of the flow can be clearly presented. A square or rectangular window was used to determine an influence region of each selected grid point. The velocity vectors in the influence region were used to conduct an statistical analysis for the selected grid point, for example, if valid vectors $\{(u_j, v_j); j=1,2,3, \dots, M\}$ were in the influence region of the n -th grid point at (x_n, y_n) , the mean velocity components were determined as

$$U_n = \frac{1}{M} \sum_{j=1}^M u_j, \quad V_n = \frac{1}{M} \sum_{j=1}^M v_j. \quad (2)$$

The mean-square velocity component fluctuations are determined as

$$\begin{aligned} \overline{uu_n} &= \frac{1}{M} \sum_{j=1}^M (u_j - U_n)^2 \\ \overline{vv_n} &= \frac{1}{M} \sum_{j=1}^M (v_j - V_n)^2 \end{aligned} \quad (3)$$

The total 2-D root-mean-square velocity fluctuations at grid point n can be quantified with

$$\delta_n = \sqrt{\overline{uu_n} + \overline{vv_n}}. \quad (4)$$

The correlation of the velocity fluctuation, i.e. the shear Reynolds stress in the xy -plane can be determined as

$$\overline{uv_n} = \frac{1}{M} \sum_{j=1}^M (u_j - U_n) \cdot (v_j - V_n). \quad (5)$$

The size of the influence region determines the spatial resolution in the final results. It should be small enough to resolve investigated flow details but large enough to accumulate a sufficient number of valid vectors for a reliable statistical analysis. In the following, a 32×64-pixel window was adopted to include enough vectors for the statistical analysis, so that mean velocities and velocity fluctuations are obtained in an area of 30×60 μm^2 .

TEST RESULTS

Test results in the center plane of the jet flow at 1.5D are given in Fig. 5. Vector maps in Fig. 5 (a) and (b) are the same. The contours in Fig. 5 (a) display the distribution of the velocity fluctuation in the test plane that indicate a root-mean-square fluctuation of 12 m/s around mean velocity of 95 m/s at the jet flow center, i.e. many of the instantaneous velocity vectors exceed 110 m/s. The contours in Fig. 5 (b) represent the distribution of shear Reynolds stress in the test plane. Both Fig. 5 (a) and (b) show that the test flow has strong turbulence, especially in the shear layers at both sides of the main jet flow. Test results at position 0.5D and 1.5D are given in Fig. 6 and Fig. 7, respectively. The three test results from 0.5D to 2.5D demonstrate the development of the shear layers of the turbulent jet flow, i.e. the thickness of the shear layer and the shear stress magnitude increase along the flow downstream, whereas the velocity fluctuation keeps the same level at the three different positions.

SUMMARY

A new configuration of MPIV is presented in this paper that extends the working distance of conventional MPIV from a few millimeters to more than 100 millimeters to make measurements of micro-scale air jet flows possible. The new MPIV system applies a zero-degree, forward-scattering optical setup, so that the laser intensity required for illuminating the sub-micron tracer particles can be minimized. The described system is equipped with an advance digital camera that has an interframing time of 180 ns, so that a much higher velocity can be measured in micro-scale tests than previously possible. The laser system has a high repeat rate, i.e. up to 30 Hz for each laser head, so that large numbers of image frames can be acquired to enable a statistical analysis of turbulent intensities. The incense smoke particles used in the current tests can easily seed the air flow with a simple air/smoke-mixer, and they scatter enough light to be imaged through the long-distance microscope with optimal diameter around 3 pixels. Experiments were conducted with a nozzle of 500 μm in diameter, which was a 8-mm long cylindrical tube. Mean velocity and turbulent distributions were determined at

three different positions of a high-speed air jet flow. The flow velocity measured in the air jet exceeded 110 m/s, and the velocity fluctuation was up to 18 m/s in the shear layer. The test demonstrates that the individual particle image tracking algorithm, the irregular median filter and irregular statistical analysis method are effective tools to evaluate a group of low-image-density PIV recording pairs.

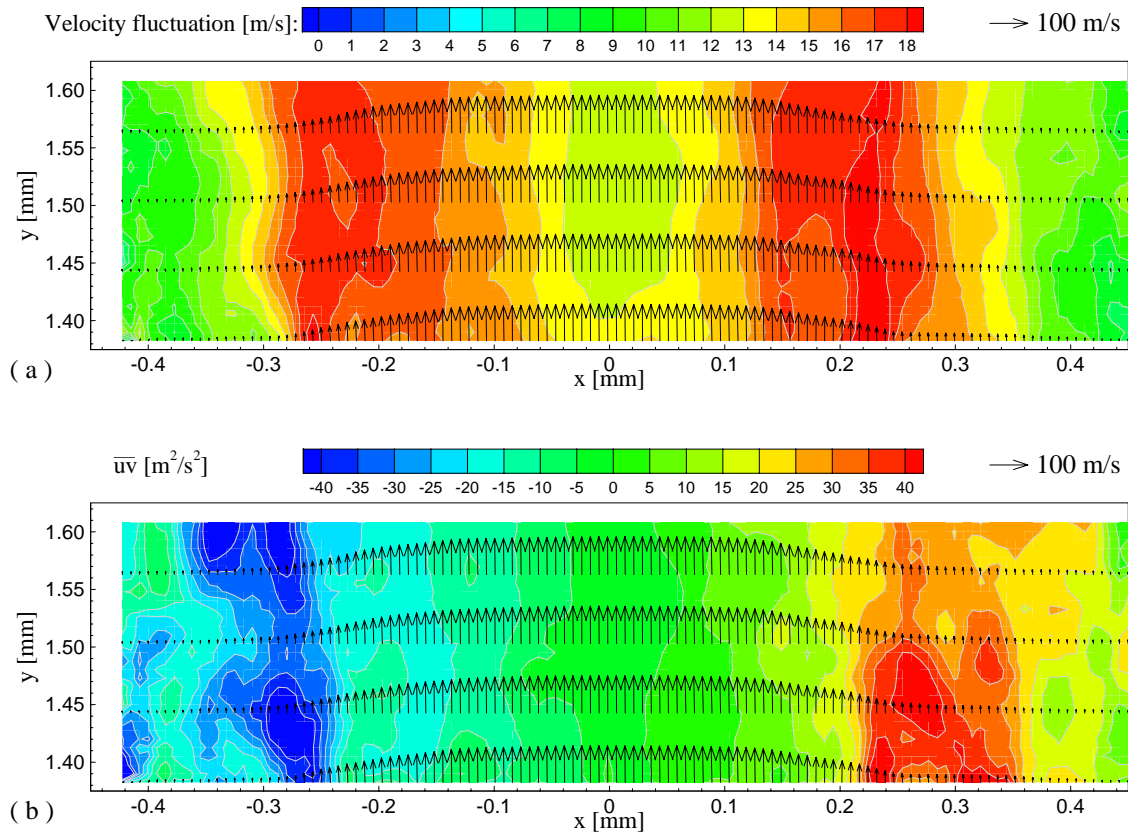


Fig. 5: Mean velocity map and turbulent value contours for test at 1.5D:

- (a) UV vectors and velocity fluctuation contours;
- (b) UV vectors and shear Reynolds stress contours.

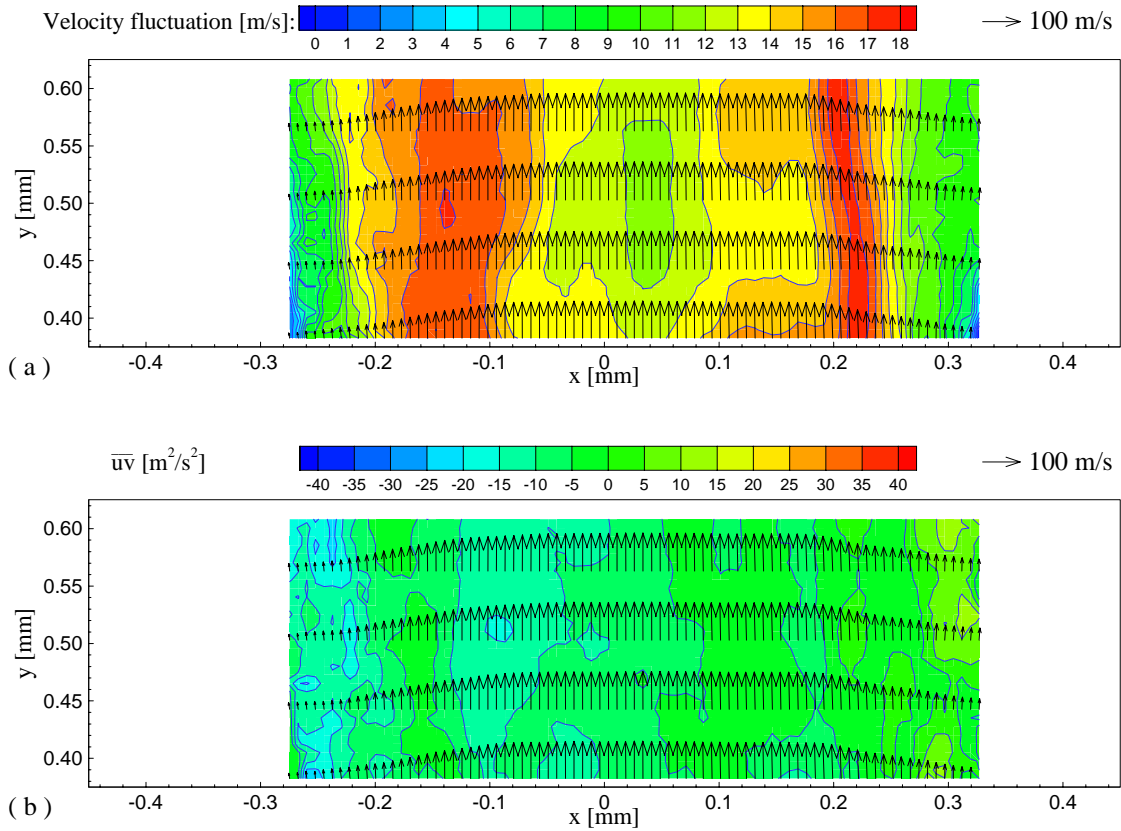


Fig. 6: Mean velocity map and turbulent value contours for test at $0.5D$: (a) UV vectors and velocity fluctuation contours; (b) UV vectors and shear stress contours.

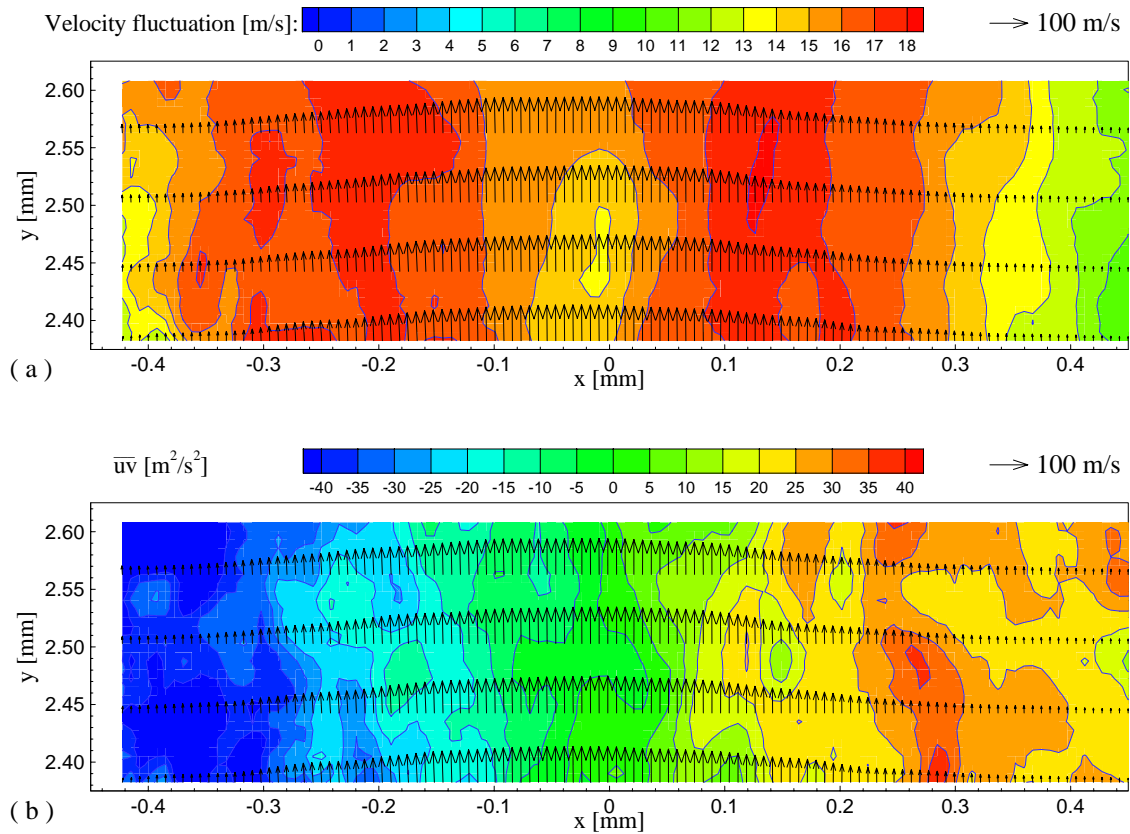


Fig. 7: Mean velocity map and turbulent value contours for test at $2.5D$: (a) UV vectors and velocity fluctuation contours; (b) UV vectors and shear stress contours.

REFERENCES

- Gui L; Merzkirch W** (1996) A method of tracking ensembles of particle images. *Exp. Fluids* 21: 465-468
- Gui L; Merzkirch W; Shu JZ** (1997) Evaluation of low image density PIV recordings with the MQD method and application to the flow in a liquid bridge. *Journal of Flow Visualization and Image Processing*, Vol. 4, No. 4, 333-343
- Gui L; Wereley ST** (2002) A correlation-based continuous window shift technique for reducing the peak locking effect in digital PIV image evaluation. *Exp. Fluids* 32: 506-517
- Lee SY; Wereley ST; Gui L; Qu W; Mudawar I** (2002) Microchannel flow measurement using micro particle image velocimetry. Intl. Mechanical Engineering Congress and Exposition, New Orleans, Louisiana, November 17-22
- Lee SY; Jang J; Wereley ST** (2004) Entrance length of Low Reynolds number flow in microchannel. *Proc. ASME/IMECE*, Paper #2004-61908, (Anaheim, CA, Nov.).
- Meinhart CD; Zhang H** (2000) The flow structure inside a microfabricated inkjet printer head. *J. Microelectromechanical Systems* 9:67-75
- Meinhart CD; Wereley ST; Santiago JG** (1999) PIV measurements of a microchannel flow. *Exp. Fluids* 27: 414-419
- Meinhart CD; Wereley ST; Santiago JG** (2000) A PIV algorithm for estimating time-averaged velocity fields. *Journal of Fluids Engineering* 122:285-289
- Meinhart CD; Santiago JG; Adrian RJ; Wereley ST** (2003) Micron Resolution Particle Image Velocimeter. US Patent 6,653,651, Nov. 25
- Santiago JG; Wereley ST; Meinhart CD; Beebe DJ; Adrian RJ** (1998) A particle image velocimetry system for microfluidics. *Exp. Fluids* 25: 316-319
- Tkaczyk E; Handa V; Lee S; McNally H; Gui L; Wereley S; Bashir R** (2002) Determination of the charge attached to micro-scale devices used in fluidic self-assembly processes. 2002 MIRS Fall Meeting, Symposium F - Nanocrystalline Semiconductor Materials and Devices, December 2 - 5, Boston, Massachusetts
- Wereley ST; Santiago JG; Meinhart CD; Adrian RJ** (1998) Velocimetry for MEMS Applications. *Proc. of ASME/DSC*, Vol. 66, (Micro-fluidics Symposium, Nov., Anaheim, CA)
- Wereley ST; Gui L; Meinhart CD** (2002a) Advanced algorithms for microscale velocimetry, *AIAA Journal*, Vol. 40, #6
- Wereley ST; Lee SY; Gui L** (2002b) Entrance length and turbulence transition in microchannels. *Amer. Phys. Soc./Div. Fluid Dyn. Annual Meeting*, Dallas, TX, November